

Magnetic Resonance Imaging and DWI Features of Orbital Rhabdomyosarcoma

Xuetao Mu^{1,2}, Hong Wang², Yueyue Li³, Yuwen Hao⁴, Chunnan Wu², Lin Ma^{1,*}

1 Department of Radiology, Chinese PLA General Hospital, Beijing 100853, China

2 Department of MRI, General Hospital of Armed Police, Beijing 100039, China

3 Institute of Orbital Disease, General Hospital of Armed Police, Beijing 100039, China

4 Computer Centre, General Hospital of Armed Police, Beijing 100039, China

Abstract

Purpose: To describe the magnetic resonance imaging (MRI) features of orbital rhabdomyosarcoma (RMS).

Methods: Thirty-nine patients with histopathologically confirmed orbital RMS were retrospectively reviewed. All patients underwent orbital conventional MRI, including axial, sagittal, and coronal T1-weighted, T2-weighted, and postcontrast T1-weighted sequences. The location, shape, margin, and MRI signal of the 39 lesions were reviewed. DWI in 15 patients and susceptibility weighted imaging (SWI) in 2 patients were also analyzed.

Results: Orbital MRI was available in 39 patients and revealed a soft tissue mass in the orbital region in all cases. Of the 39 patients, the primary tumor sites were limited to the orbital proper in 31 cases, while 28 cases had extraocular muscle invasion and 8 cases had extraorbital invasion. All lesions were unilateral. Thirty-three cases were well-defined soft tissue masses and 6 cases appeared as less well-defined soft-tissue masses. Thirty-four cases showed homogeneous isointense or slightly hypointense signals on T1-weighted imaging (T1WI) and hyperintense signal on T2-weighted imaging (T2WI) compared with extraocular muscles. Five cases had heterogeneous signals with focal areas of increased signal on T1WI or decreased signal on T2WI, including 1 case with hypointense signal on SWI. The mean apparent diffusion coefficient (ADC) value of the viable part of tumors was $(0.925 \pm 0.09) \times 10^{-3} \text{ mm}^2/\text{s}$. All cases showed moderate to marked enhancement after contrast administration.

Conclusion: Several MRI features-including homogeneous

isointense or slightly hypointense signal on T1WI and slightly hyperintense signal on T2WI, relative low ADC values, and moderate to marked enhancement, extraocular muscles invasion, and extraorbital extension are helpful in the diagnosis of orbital RMS. (*Eye Science 2014; 29: 6–11*)

Keywords: orbit; Rhabdomyosarcoma; Magnetic resonance imaging; Diffusion-weighted imaging; susceptibility weighted imaging

Abbreviations: ADC: Apparent diffusion coefficient; BW: Band width; CT: Computer tomography; DWI: Diffusion-weighted imaging; FA: Flip angle; FOV: Field of view; MRI: Magnetic resonance imaging; RMS: Rhabdomyosarcoma; SWI: Susceptibility weighted imaging; TE: Time echo; TR: Time repetition; T1WI: T1-weighted imaging; T2WI: T2-weighted imaging

Introduction

Rhabdomyosarcoma (RMS) is the most common soft tissue sarcoma and primary orbital malignancy in childhood. The annual incidence of RMS is approximately 4.5 cases per million in children. The head and neck region is the most frequent site, accounting for 35–40% of all cases^{1,2}. In children, orbital RMS accounts for 25–35% of the head and neck soft tissue malignant tumors^{3,4}. Since RMS is a life-threatening malignant tumor, proper and early diagnosis is of great importance in saving the lives of patients. However, RMS does not have specific clinical manifestations, which make it difficult to diagnose clinically in preoperative evaluation.

The advancements in neuroimaging techniques have led to magnetic resonance imaging (MRI) be-

DOI: 10.3969/j.issn.1000-4432.2014.01.002

Declaration: The authors report no conflicts of interest.

* **Corresponding author:** Lin Ma, E-mail: cjr.malin@vip.163.com

coming a powerful tool in the diagnosis of orbital RMS. However, literature searches on RMS reveal that most reports focus on the patient's clinical spectrum or life prognosis after various treatments; only a few case reports have described the MRI findings of orbital RMS⁵⁻⁸. In these case reports, which have very small sample sizes, the main MRI finding for orbital RMS was a soft tissue mass with moderate to marked contrast enhancement. Little description was provided for the diagnostic features, nor were new MRI techniques applied, such as diffusion weighted imaging (DWI) and susceptibility weighted imaging (SWI). Thus, detailed MRI features of RMS are scarce.

The goal of this study was to describe and define the clinical, imaging, and pathological changes of RMS, with particular emphasis on the various MRI features including structure, DWI, and SWI.

Materials and methods

This study was approved by the institutional review board, and the clinical records and MRI data of 39 consecutive patients with histologically proven RMS over a 5-year period (from October 2007 to November 2012) were retrospectively reviewed.

All patients underwent orbital conventional MRI before surgery. MRI was performed on a 3.0 T scanner (TRIO TIM, Siemens Medical Systems) with a SENSE 8-channel head coil. In total, 17 children required sedation for MRI. Chloral hydrate was used under a standard sedation protocol with direct supervision by a research nurse until each child had returned to baseline state. Conventional clinical pulse sequences were used, including axial, sagittal, and coronal T1-weighted fast low-angle shot sequences [slice thickness=3 mm, intersection gap=0.3 mm, slice number=19, time repetition (TR)/time echo (TE)=1900/2.5 ms, field of view (FOV)=190×190 mm, band width (BW)=269 Hz, flip angle (FA)=70°], and axial, sagittal, and coronal T2-weighted turbo spin echo sequences (slice thickness=3 mm, intersection gap=0.3 mm, slice number=19, TR/TE=3300/108 ms, FOV=190×190 mm, BW=363 Hz, flip angle=140°).

DWI measurement was performed in the axial plane using a SE-EPI sequence and b-values of 0, 500, and 1000 s/mm² (slice thickness=3 mm, inter-

section gap=0.3 mm, slice number=19, TR/TE=3200/99 ms, FOV=190×190 mm, BW=1240 Hz) in 15 patients.

SWI measurement was performed in the axial plane using a three-dimensional gradient recalled echo sequence (slice thickness=1.2 mm, slice number=128, TR/TE=28 ms/20 ms, FOV=220×220 mm, flip angle=15°, matrix=512×512) in 2 patients.

Postcontrast axial, sagittal, and coronal T1-weighted imaging (T1WI) with fat saturation was acquired with the same parameters as the precontrast T1WI in all patients. Gadopentetate Dimeglumine (Bayer Schering Pharma AG, Berlin, Germany) was intravenously injected at a dose of 0.1 mmol/kg of body weight.

MR images were reviewed on a Siemens parallel processing workstation by 3 radiologists (HW, XTM, and CNW with 22, 10, and 5 years of working experience, respectively), and consensus was reached by discussion.

Results

The patients enrolled in the study included 22 females (56.4%) and 17 males (43.6%). The median age was 7 years (age ranged from 2 to 38 years). The disease course ranged from 10 to 90 days (mean 30.80±18.78 days). All 39 patients underwent surgical removal of the lesions, and 6 of them had relapses after operation. All the recurrent patients underwent secondary surgery or radiation therapy. The common symptoms were as follows: progressive proptosis (33 patients, 84.6%), globe displacement (25 patients, 64.1%), conjunctival and eyelid swelling (19 patients, 48.7%), blepharoptosis (14 patients, 35.9%), palpable mass (10 patients, 25.6%), and pain (4 patients, 10.3%).

Orbital MRI was available in 39 patients and revealed a soft tissue mass in the orbital region in all cases. All the lesions were unilateral. The involved side was the right side in 20 cases (51.3%) and the left side in 19 cases (48.7%). The lesions showed a well-defined margin in 33 cases (84.6%) and ill-defined in 6 cases (15.4%). Of the 39 patients, the primary tumor site was limited to the orbital proper in 31 cases (79.4%); 28 showed extraocular muscle invasion (71.8%). Sinus invasion by the orbital tumor was found in 5 cases (12.8%; maxillary sinus in

3 cases, ethmoidal sinus in 1 case; involvement in both ethmoidal and nasal sinus in 1 case). Intracranial invasion was detected in the remaining 3 cases (7.7%) (Figure.1). In all, 34 cases showed homogeneous isointense or slightly hypointense signals on T1WI and hyperintense signal on T2WI compared with the signals of extraocular muscles(87.2%). Five cases had heterogeneous signals with focal areas of increased signal on T1WI and decreased signal on T2WI, including 1 case with hypointense signal on SWI, indicating chronic or subacute hemorrhage (12.8%) (Figure 2). DWI showed a hyperintense signal in 15 cases and the mean apparent diffusion coefficient (ADC) value of the solid part of the 15

lesions was $(0.925\pm 0.09)\times 10^{-3} \text{ mm}^2/\text{s}$ (Figure 3). All cases showed moderate to marked enhancement after contrast administration (100%).

Two cases were misdiagnosed as capillary hemangioma and 1 case was misdiagnosed as lymphangioma before operation, and triamcinolone acetonide injection was given to these patients. After treatment, however, the lesions increased significantly. RMS was diagnosed after tumor resection.

Typical histopathological features were confirmed in 32 cases(82.1%). Seven cases only showed histopathological features of malignant small cell tumors, and were ultimately confirmed as RMS by immunohistochemistry study (17.9%).

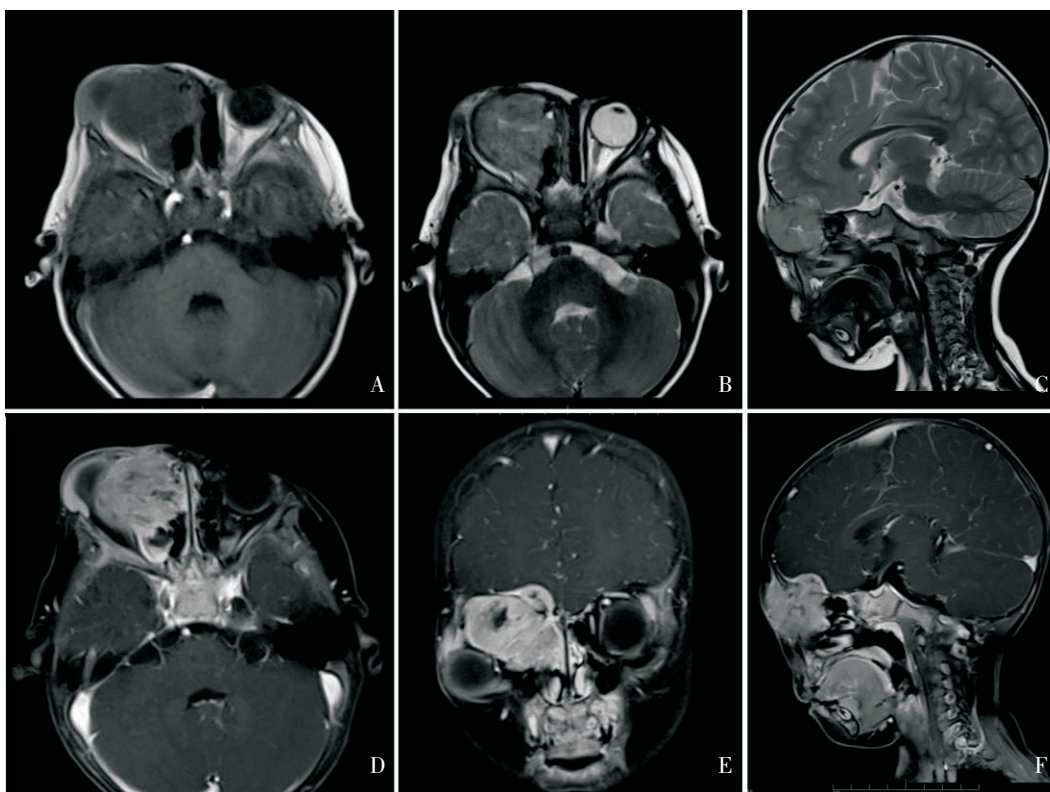


Figure 1 A 2-year-old boy with embryonal rhabdomyosarcoma with ethmoidal sinus and intracranial invasion. Figure 1A-C: Axial T1WI, T2WI and sagittal T2WI demonstrated a superonasal lesion in the right orbit with ethmoidal sinus and intracranial invasion. Figure 1D-F: The lesion and the invaded meninges showed marked heterogeneous enhancement on postcontrast axial, coronal, and sagittal T1WI with fat saturation.

Discussion

RMS is the most common primary orbital malignant tumor in children, occurring primarily in patients from age 2 to 10. However, the tumor could occur at any age from birth to adulthood, even up to

78 years of age^{2,4}. The oldest patient in this study was 38 years of age. Clinically, orbital RMS usually presents with a spectrum of non-specific symptoms, including painlessly and rapidly progressing unilateral proptosis, eyelid edema, conjunctival congestion, and blepharoptosis, *etc*. It is difficult to arrive at a

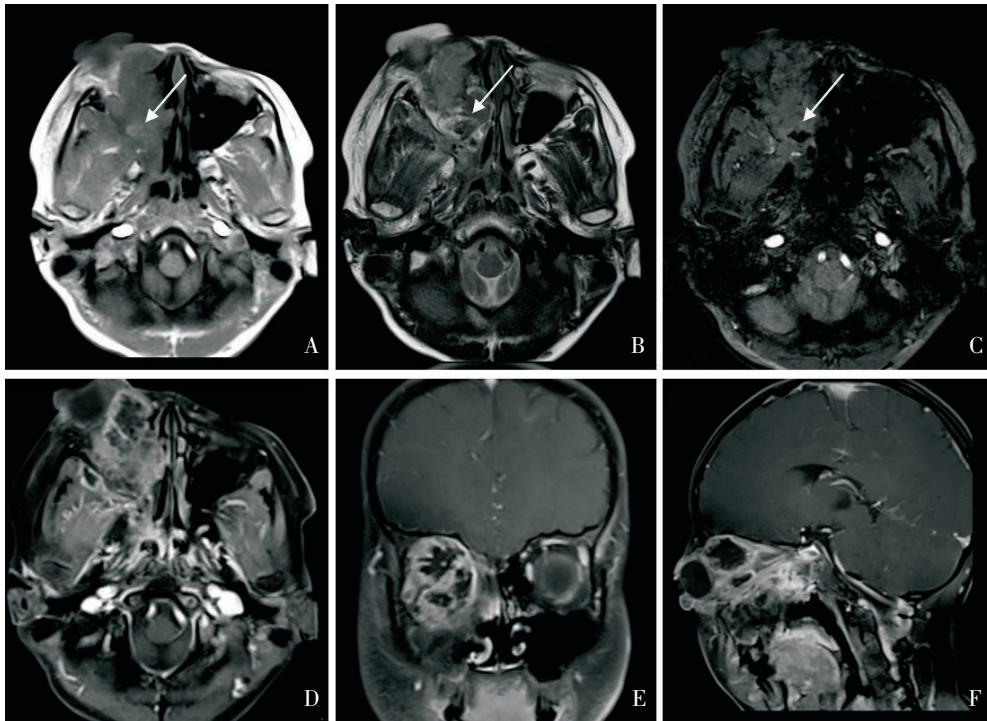


Figure 2 A 10-year-old boy with heterogeneous rhabdomyosarcoma with nasal invasion. Figure 2A-B: Axial T1WI and T2WI demonstrated a lesion with heterogeneous signals with focal areas of increased signal on T1WI and decreased signal on T2WI (arrow). The lesion also showed nasal invasion. Figure 2C: The lesion showed focal areas with hypointense signal on SWI (arrow). Figure 2D-F: The lesion showed heterogeneous enhancement on postcontrast axial, coronal, and sagittal T1WI with fat saturation.

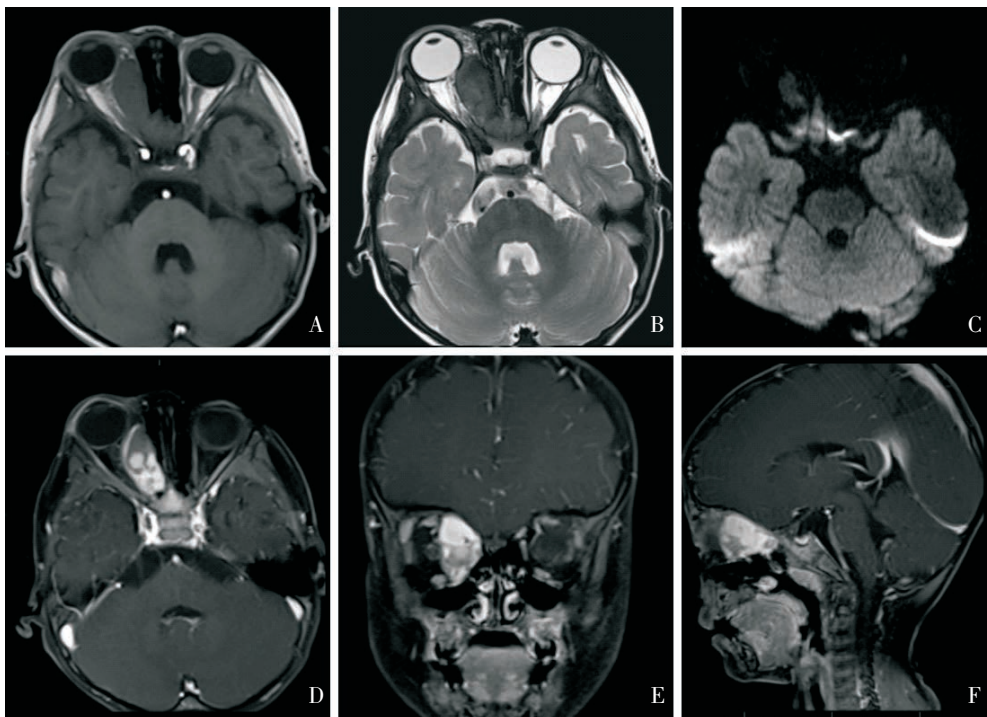


Figure 3 A 2-year-old boy with embryonal rhabdomyosarcoma. Figure 3A: Axial T1WI demonstrated an oval extraconal lesion in the right orbit with an isointense signal relative to the muscle. Figure 3B: The lesion showed a heterogeneously hyperintense signal on T2WI. Figure 3C: The lesion showed a hyperintense signal on DWI ($b=1000$). Figure 3D-F: The lesion showed a marked heterogeneous enhancement on postcontrast axial, coronal, and sagittal T1WI with fat saturation.

correct diagnosis purely based on clinical manifestations.

MRI was crucial in the preoperative evaluation of orbital RMS, especially in determining the tumor location and margin, and in evaluating the residual or recurrent lesions. Orbital RMS presents some MRI characteristics. On T1WI, the tumor may appear as an isointense to hypointense signal compared with the extraocular muscles. On T2WI, RMS tumor can present as a hyperintense, isointense, and even hypointense signal with respect to both extraocular muscles and orbital fat. On postcontrast T1WI, RMS shows moderate to marked enhancement. In some cases, especially in children under two years of age, a highly vascular internal architecture with marked enhancement, mimicking a capillary hemangioma, may be seen, and it can be easily misdiagnosed. When RMS presents bone erosion and intracranial extension, special attention should be paid because it necessitates different operation access^{9,10}. In our study, 8 patients had sinus, intracranial, and bone invasion, and MRI clearly showed the scope of extension.

DWI is sensitive to the histological and physiological status of tumors and can be helpful in the differential diagnosis. Some authors suggest that ADC values may provide quantitative information that was useful for differentiating between the benign (mean ADC value= $1.57 \pm 0.33 \times 10^{-3} \text{ mm}^2/\text{s}$) and malignant lesions (mean ADC value= $0.84 \pm 0.34 \times 10^{-3} \text{ mm}^2/\text{s}$) in the orbit; the threshold value for differentiating malignant orbital tumors from benign lesions was $1.15 \times 10^{-3} \text{ mm}^2/\text{s}$ ^{11,12}. The 15 lesions in the present study showed relatively low ADC values (mean ADC value= $0.925 \pm 0.09 \times 10^{-3} \text{ mm}^2/\text{s}$), which was consistent with the malignant lesions.

SWI provides a new means to enhance contrast. It is three to six times more sensitive than conventional T2*-weighted gradient-echo sequences in determining the size, number, volume, and distribution of intratumoral hemorrhages, and it is also more specific in differentiating the hemorrhage from other similar lesions and artifacts^{13,14}. In this study, 2 cases underwent SWI measurement. One case had heterogeneous signals with focal areas of increased signal on T1WI and decreased signal on T2WI, and showed

central hypointense signal on SWI, which was defined as intratumoral hemorrhage.

RMS should be differentiated from other lesions in the orbit, including orbital cellulitis, idiopathic inflammatory orbital pseudotumor, capillary hemangioma, lymphangioma, Langerhans' cell histiocytosis, dermoid cyst, *etc.* Most of those conditions can be differentiated by clinical history and MR examination. Orbital cellulitis is more common than RMS, and usually shows sinus and orbital inflammation, and subperiosteal abscess near the medial wall of the orbit. A DWI sequence with parallel acquisition should improve the diagnostic confidence¹⁵. Idiopathic inflammatory orbital pseudotumor generally shows more inflammatory signs, including enlargement of the muscle, a finding that would be highly unlikely in RMS. A trial of corticosteroids is helpful in differentiating between idiopathic orbital inflammation and RMS¹⁶. Orbital capillary hemangioma generally appears in infants during the first few months of life, and it generally presents with a slow growing feature¹⁷. Orbital lymphangioma frequently reveals blood levels in the larger cystic spaces that comprise the mass. These hemorrhagic cysts would be unlikely in RMS¹⁸. Langerhans' cell histiocytosis generally arises in bone and produces atypical bony destruction, which would be rare in orbital RMS¹⁹. Dermoid cyst usually locates near the superotemporal orbital rim. MRI characteristically shows a cystic component and no enhancement.

Based on its histopathological characteristics, RMS can be categorized into different subtypes. For most RMS cases, the subtype of tumor can be determined by pathological examination after surgery. For a small number of cases, diagnosis of the subtype can be difficult because of the overlap of pathological characteristics among different subtypes. In this study, 32 cases were diagnosed as orbital RMS by histopathological characteristics. For the remaining 7 cases, the tumors were initially diagnosed as small cell tumors by histopathological characteristics, and were ultimately confirmed as RMS by immunohistochemistry.

In conclusion, RMS is the most common primary orbital malignancy in children and can be evaluated and diagnosed by MRI. Several important MRI fea-

tures should be considered to better understand the disease, which include rapidly developing unilateral proptosis in childhood, well-demarcated homogeneous soft tissue masses with extraocular muscle invasion, isointense or slightly hypointense signals on T1WI, hyperintense signals on T2WI, relatively low ADC values, and moderate to marked enhancement.

References

- 1 MacArthur CJ, McGill TJ, Healy GB. Pediatric head and neck rhabdomyosarcoma. *Clinical pediatrics*, 1992 Feb, 31 (2):66–70.
- 2 Karcioğlu ZA, Hadjistilianou D, Rozans M, et al. Orbital rhabdomyosarcoma. *Cancer Control; Journal of the Moffitt Cancer Center*, 2004 Sep-Oct, 11(5):328–333.
- 3 Mafee MF, Pai E, Philip B. Rhabdomyosarcoma of the orbit. Evaluation with MR imaging and CT. *Radiologic Clinics of North America*, 1998 Nov, 36(6):1215–1227.
- 4 Shields JA, Shields CL. Rhabdomyosarcoma: review for the ophthalmologist. *Survey of Ophthalmology*, 2003 Jan-Feb, 48(1):39–57.
- 5 Mendez Mdel C, Muinos Y, Blanco G, et al. Embryonal rhabdomyosarcoma of the caruncle in a 4 year-old boy: case report. *Arquivos Brasileiros de Oftalmologia*, 2012 May-Jun, 75(3):207–209.
- 6 Tsuchisaka A, Usui Y, Goto H, et al. Two cases of orbital embryonal rhabdomyosarcoma with chromosome aberration. *Nippon Ganka Gakkai Zasshi*, 2010 Apr, 114(4):374–380.
- 7 Kaliaperumal S, Tiroumal S, Rao V. Orbital rhabdomyosarcoma: a case series. *Indian Journal of Cancer*, 2007 Jul-Sep, 44(3):104–107.
- 8 Mulugeta A, Bejjiga A, Bezabih K. Embryonal rhabdomyosarcoma of the orbit in a 38-year-old woman. *Ethiopian Medical Journal*, 2001 Jan, 39(1):47–51.
- 9 Judmaier W, Birbamer G, Buchberger W, et al. MR imaging of late onset orbital rhabdomyosarcoma with intracranial extension. *Magnetic Resonance Imaging*, 1993, 11 (2):285–288.
- 10 Das JK, Tiwary BK, Paul SB, et al. Primary orbital rhabdomyosarcoma with skeletal muscle metastasis. *Oman Journal of Ophthalmology*, 2010 May, 3(2):91–93.
- 11 Razeq AA, Elkhamary S, Mousa A. Differentiation between benign and malignant orbital tumors at 3-T diffusion MR-imaging. *Neuroradiology*, 2011 Jul, 53(7):517–522.
- 12 Lope LA, Hutcheson KA, Khademian ZP. Magnetic resonance imaging in the analysis of pediatric orbital tumors: utility of diffusion-weighted imaging. *Journal of AAPOS; the official publication of the American Association for Pediatric Ophthalmology and Strabismus/American Association for Pediatric Ophthalmology and Strabismus*, 2010 Jun, 14(3):257–262.
- 13 Lobel U, Sedlacik J, Sabin ND, et al. Three-dimensional susceptibility-weighted imaging and two-dimensional T2*-weighted gradient-echo imaging of intratumoral hemorrhages in pediatric diffuse intrinsic pontine glioma. *Neuroradiology*, 2010 Dec, 52(12):1167–1177.
- 14 Barnes SR, Haacke EM. Susceptibility-weighted imaging: clinical angiographic applications. *Magnetic resonance imaging clinics of North America*, 2009 Feb, 17(1):47–61.
- 15 Sepahdari AR, Aakalu VK, Kapur R, et al. MRI of orbital cellulitis and orbital abscess: the role of diffusion-weighted imaging. *American Journal of Roentgenology*, 2009 Sep, 193(3):W244–250.
- 16 Ding ZX, Lip G, Chong V. Idiopathic orbital pseudotumor. *Clinical radiology*, 2011 Sep, 66(9):886–892.
- 17 Kavanagh EC, Heran MK, Peleg A, et al. Imaging of the natural history of an orbital capillary hemangioma. *Orbit*, 2006 Mar, 25(1):69–72.
- 18 Bilaniuk LT. Vascular lesions of the orbit in children. *Neuroimaging Clinics of North America*, 2005 Feb, 15(1):107–120.
- 19 Maccheron LJ, McNab AA, Elder J, et al. Ocular adnexal Langerhans cell histiocytosis clinical features and management. *Orbit*, 2006 Sep, 25(3):169–177.